

Signature of Transition between Granular Solid and Fluid: Rate-Dependent Stick Slips in Steady Shearing

Jih-Chiang (JC) Tsai^{1,*}, Guan-Hao Huang¹, and Cheng-En Tsai^{1,2}

¹*Institute of Physics, Academia Sinica, 11529 Taipei, Taiwan*

²*Department of Physics, National Central University, 320317 Chung-Li, Taiwan*

 (Received 15 February 2020; revised 4 November 2020; accepted 28 January 2021; published 23 March 2021)

Despite extensive studies on either smooth granular-fluid flow or the solidlike deformation at the slow limit, the change between these two extremes remains largely unexplored. By systematically investigating the fluctuations of tightly packed grains under steady shearing, we identify a transition zone with prominent stick-slip avalanches. We establish a state diagram, and propose a new dimensionless shear rate based on the speed dependence of interparticle friction and particle size. With fluid-immersed particles confined in a fixed volume and forced to “flow” at viscous numbers J decades below reported values, we answer how a granular system can transition to the regime sustained by solid-to-solid friction that goes beyond existing paradigms based on suspension rheology.

DOI: [10.1103/PhysRevLett.126.128001](https://doi.org/10.1103/PhysRevLett.126.128001)

Granular-fluid mixtures, ranging from natural phenomena such as quicksand, debris flows, landslides, to grains in industrial mixers and silos, are excellent examples exhibiting solid-fluid duality. On one hand, smooth flows as a dense suspension have been successfully described by the paradigm of “ J rheology” [1] with viscous numbers J down to the order of 10^{-5} . On the other hand, flows of tightly packed grains have been treated by a separate tradition with elastoplastic models and theories [2]. Understanding the transition between these two extremes remains a profound challenge, not only in complexity of partial fluidizations [3–5], but also due to the lack of experimental observations on such transitions [6]. Two recent narratives since the initial proposal of the jamming phase diagram [7] have been that the “jamming point” depends on interparticle friction [8], and that friction makes granular systems go beyond “ideal jamming” (with isotropic compression) and exhibit fragile states where the role of shearing becomes explicit [9–12]. Several experiments [13–15] and numerical studies [16] have demonstrated that friction plays a decisive role in creating a dramatic change of behaviors.

Numerous prior works focus their attention on either rapid flows of suspension [13–15] or “quasistatic” systems [9,12], leaving the transition in between largely unexplored. In reality, “friction coefficient” can vary substantially with the driving rate, and speed-dependent frictions have long been considered the root of instabilities leading to catastrophic consequences like earthquakes [17–19]. However, despite the ongoing debates over the mechanism behind the rate-dependent jamming in rapid flows, also known as discontinuous shear thickening [13–16,20–22], roles of the speed dependence of friction on slow flows of tightly packed grains such as quicksand, steady flows in an hourglass, and their regime transition appear missing from

existing discussions [6]. Recent studies have reported hysteresis and nonmonotonic flow curves in experiments with frictional particles [23,24]. But without systematically looking into fluctuations, the *dynamics* behind the solid-fluid transition remains elusive.

In this Letter, we begin with showing a “dangerous zone” of driving rates that exhibits prominent stick-slip avalanches for packed grains sheared in a fixed volume. Such a transition zone bridges the gap between the solidlike regime in the “slow” extreme and smooth flows on the faster side. Its occurrence is linked to the speed-dependent friction between particles, which we determine by direct measurements. The avalanche is interpreted as the consequence that low-friction contacts get a chance to percolate through a network of load-bearing particles and induce repetitive landslides. We establish a state diagram that connects different flow regimes, and propose a new dimensionless shear rate based on the interparticle tribology. Our work shows how the existing paradigm of J rheology experiences its transition, as we create shear flows that are three decades below reported values of J and reach the regime of granular solids.

Setup and overview of transitions.—Shown as in Fig. 1(a), our particles fill the space between two cones. The sidewall is formed by a stack of free-sliding acrylic rings with an inner diameter $2R = 22$ cm. Two cones are geometrically roughed at the scale of the particle with diameter $d \approx 9$ mm. The upper cone is set at a fixed height, with the mechanism specially reinforced to provide a smooth rotation at an angular resolution of $2\pi \times 10^{-4}$ with a wide range of angular speeds Ω . The base of the system is supported by the arrangement of six independent force sensors, in order to determine the total forces and moments that keep the base stationary. The gap between the rotating

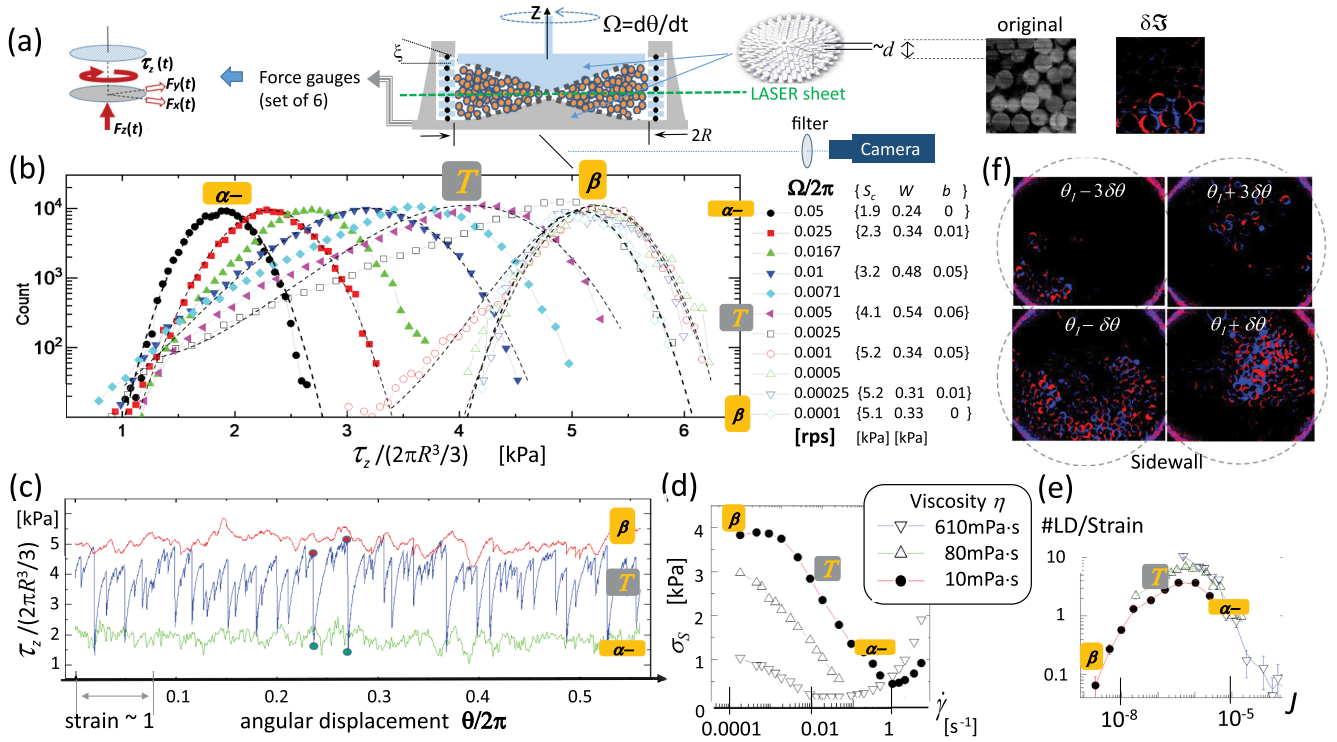


FIG. 1. (a) Schematics for the setup and measurements, from left to right: the time-dependent torque and three net forces as determined from sensors around the base; cross-sectional view of the main setup (with a stack of acrylic rings alternating with ball bearings to minimize resistance along θ); 3D illustration of the roughened cones; close-up of a typical fluorescent image; and the differential image δS computed from two frames with $\delta\theta = 8\pi \times 10^{-4}$. (b) Statistical distributions of torque τ_z measured over time, at different rotation rates $\Omega/2\pi$ (in revolutions per second, rps) denoted by symbols. Dashed lines show curves $\sim \exp\{-0.5[(S - S_c)/W]^2 - b[(S - S_c)/W]^3\}$, where $S \equiv \tau_z/(2\pi R^3/3)$ with empirical fit parameters indicated on the graph $\varphi = 0.60$. (c) Time series of S for three states in (b), all plotted against the angular displacement, which can also be converted to effective strain $\equiv \Omega t/2 \tan \xi$. The high-frequency noises are smoothed by 40 ms. (d) Time-averaged stress σ_s , plotted against the shear rate $\dot{\gamma} \equiv \Omega/2 \tan \xi = 13.7(\Omega/2\pi)$. (e) Counts of LD per unit strain, plotted against the viscous number J , as defined in main texts. Data in (d) and (e) involve experiments with three different viscosity η in the fluid, at the same $\varphi = 0.56$. (f) Sequence of differential images δS with $\delta\theta = 2\pi \times 10^{-4}$, accompanying one of the large stress jumps in state T . Pixels in positive (negative) values are displayed in blue (red). The boundary movement $\theta(t)$ is indicated in reference to a fixed θ_1 .

boundary and the sidewall is 2 mm such that all particles cannot escape. The nominal volume fraction is defined as $\varphi = N v_1/V_{\text{access}}$ in which $N = O(1000)$ is the number of particles. V_{access} represents the total volume accessible by the particles, and v_1 stands for the volume for the single particle (which has been determined by Archimedes' method and checked for the monodispersity). Simultaneously, we take internal images of particles via the bottom, when the interstitial space is filled with aqueous solution of 60% glycerol such that the refractive index is matched to the particles [25,26]. We illuminate the system at its midheight, with a horizontal laser sheet at the wavelength of 532 nm going through the 1 mm gap between the tips of two cones. Image contrasts are generated by dyeing either particles or the fluid with rhodamine. Data reported in this Letter are based on spherical particles of polydimethylsiloxane (PDMS) elastomer that we create by molding, with the standard curing agent provided by the manufacturer [27]. We have

verified that particles exhibit a Hertzian response to compression with a Young's modulus around 1.5 MPa, which is *soft* relative to the rigidity of our driving mechanism—see Appendixes A and C in Supplemental Material [28] for further details.

To demonstrate the continuous change of behaviors, Fig. 1(b) shows the time histogram of instantaneous torque τ_z (presented as an effective stress), for experiments at a wide range of driving rates (in revolutions per second, rps) sharing the same volume fraction. At either the fast or the slow end, the histogram presents a bell shape. Note that the slower runs are at the state of *higher* stress, in startling contrast with reported studies on most rheometric flows [21,22,34]. Interestingly, between the two extremes, histograms are highly asymmetrical (as shown by the parameter b). The case at 0.005 rps is labeled as state T . The extreme case with a relatively high (or low) stress is labeled as state β (or $\alpha-$) to facilitate subsequent discussions. Time series of τ_z for these three states are compared in Fig. 1(c).

One might also time average the τ_z , define a mean stress σ_S , and plot it against the shear rate $\dot{\gamma} \equiv \Omega/2 \tan \xi$: shown as in Fig. 1(d), the behaviors mimic the nonmonotonic “flow curves” as those reported by Ref. [24]. Note that Fig. 1(d) cover data from experiments at a wider range of driving rates than those in Fig. 1(b), plus two additional runs with interstitial fluids at higher viscosities (by increasing the concentration of glycerol). The mean stress shows not only an interval of negative slope over $\dot{\gamma}$, but also an uprising across its minimum. As a rough indicator for the occurrence of stick slips, we compute the normalized counts of large drops that we refer as LD, that is defined as a sudden drop of torque larger than twice the root-mean-square of the total fluctuation—see Appendix B in Supplemental Material [28]. Results are plotted in Fig. 1(e) against the viscous number [1] $J \equiv \eta \dot{\gamma} / \sigma_N$ which incorporates our normal-stress measurements $\sigma_N \equiv$ time-averaged $F_z / \pi R^2$. The data show a consistent rise and fall over the change of J .

Stick-slip avalanches and the slow extreme.—The change from state T to state β deserves special attention. In Fig. 2, we show the cumulative distributions of stress drops as functions of a variable threshold Δ_{\min} : for each driving rate, we count the number of sudden drops in torque ($-\Delta\tau_z$) that are larger than Δ_{\min} , normalized by the total strain, and plot the

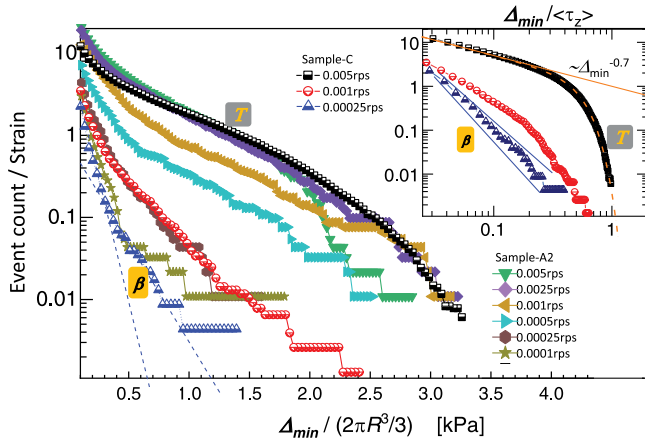


FIG. 2. Cumulative distribution of torque (stress) drops with $-\Delta\tau_z > \Delta_{\min}$, for experiments at different driving rates (rps). Event counts are normalized by the strain accumulated. Data cover experiments using two batches of particles (A2 and C) in the same fluid. $\varphi = 0.56$. In the inset, Δ_{\min} is normalized by the mean $\langle\tau_z\rangle$ for each driving rate, while logarithmic slopes of -0.7 , -2.5 , and -3 are indicated by straight lines and a truncated power law $\sim\{(\Delta_{\min}/\langle\tau_z\rangle)^{-0.7} \exp[-(\Delta_{\min}/\langle\tau_z\rangle)/0.54]\}^{2.8}$ by the dash-dotted curve—see Appendix D in Supplemental Material [28] for further analyses. In the main plot, two dotted lines illustrate exponential decays with the characteristic stress being 0.2 and 0.4 kPa, respectively. Although statistics from the two batches of particles do not coincide exactly in terms of the corresponding revolutions per second (due to different histories of immersion—see Appendix C3 in Supplemental Material), the general trend over the wide range of driving rates is consistent.

normalized counts against Δ_{\min} . The results characterize the change of behaviors in a quantitative manner.

For state T , we use the inset to highlight that the *small* avalanches resemble a power-law distribution up to about 40% of the mean torque $\langle\tau_z\rangle$. This can be translated into a probability density $\sim|\Delta\tau_z|^{-1.7}$. It is worth noting that observations of power laws can be traced back to centuries of earthquake observations, known as Gutenberg-Richter law showing a power-law distribution on released energy $\sim E^{-\tau_0}$ extending for several decades: reported values of τ_0 range from 1.8 to 2.2 depending on geography, and are reproduced by numerical models in different degrees of conservation [35]. In terms of stress release, mean-field-theory prediction has a long tradition back to half a century ago and $\tau_0 = 3/2$ is commonly seen [36].

On the other hand, *larger* avalanches deviate strongly from power law and show a stronger-than-exponential truncation—see dashed line and the description in caption. This suggests that large slips represent different physics from small ones. (Similar distinctions have been discussed over classic studies on sand piles in terms of system-spanning displacements versus localized failures [37].) Quantitatively, the statistics show that stress drops larger than 1 kPa (that corresponds to $\sim 0.3\langle\tau_z\rangle$) can occur several times within a shear strain of unity. Readers are encouraged to watch online movies in Supplemental Material [28] that reveal sudden, system-spanning displacements of particles upon these stress drops—Fig. 1(f) shows four snapshots around one such event. Also available online are animations based on the multi-component force measurements: for state T , (a) the animated τ_z - F_z plot reveals multiple “loading curves” that are often terminated by a slip event. Meanwhile, (b) the scattered plot of the net force F_y - F_x shows “clusters” during the stress buildups and sudden “jumps” in between [28].

For state β , one might see the granular pack as mostly in the *stick* mode, at a relatively high level of stress. The system “flows” in the form of small, isolated avalanches—see movies in Supplemental Material [28] for their spatial sizes and vivid demonstrations of “dynamical heterogeneities” [38]. Statistically, Fig. 2 shows that the stress drop above 1 kPa would be *extremely rare*: it takes a shear strain $\sim 10^2$ (corresponding to about three days in our laboratory experiments) to accumulate one. Such rareness indicates the lack of opportunities to “reset” the grain configurations and explains why state β displays a higher mean stress than that of state T . Recalling the time distribution of τ_z [Fig. 1(b)], it is also important to point out that even though state β displays a bell shape resembling that of state α , the two states are dominated by qualitatively different physics. As a result, at precisely the same volume fraction, the time-averaged σ_S is not only higher at state β but also shows a plateau, as seen from Fig. 1(d) and our further elaboration below.

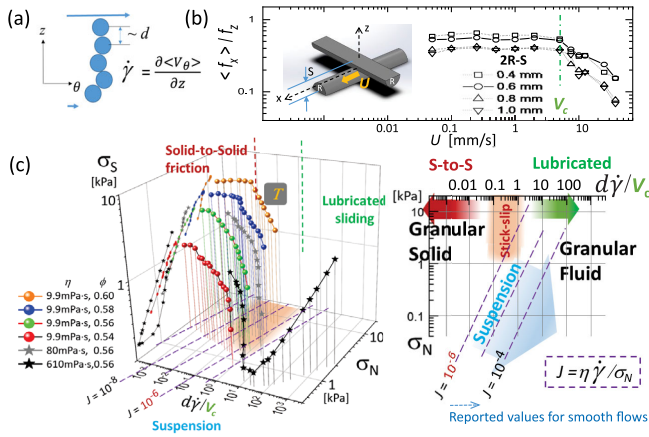


FIG. 3. (a) Illustration of the motion of densely packed particles under an imposed shear rate $\dot{\gamma}$; (b) schematics and results of measurements on the average tangential force f_x , normalized by the normal force f_z , for a localized contact between PDMS surfaces with a radius of curvature R . Data are plotted as functions of the sliding speed, for experiments at multiple pressing depths (controlled by the distance S between the base planes) up to about $0.1d$. Data reveal a critical velocity V_c that appears insensitive to the pressing depth $2R-S$. (c) State diagram summarizing data from experiments with different values of ϕ and η . On the main graph, the vertical coordinate shows the time-averaged shear stress σ_S , plotted against the dimensionless shear rate $d\dot{\gamma}/V_c$ and the normal stress σ_N . On the right, we display a schematic projection onto the $\sigma_N - d\dot{\gamma}/V_c$ plane, with contours of constant viscous number J represented by dashed lines indicating 10^{-4} , 10^{-6} , and in turn to values as small as 10^{-8} back on the main graph. Reported values of J are based on Ref. [1].

Connection with tribology and a state diagram for solid-fluid transition.—These rate-dependent behaviors can be consistently explained by first considering two facts. (1) Illustrated as Fig. 3(a), imposing a shear rate $\dot{\gamma}$ to a densely packed system creates a range of relative speeds among particles. In a system that is strongly damped, the anticipated distribution should be around the most probable speed $\sim d\dot{\gamma}$. (2) By independent measurements using the same fluid and PDMS elastomer with a radius of curvature $R = d/2$ to mimic our main experiments, we characterize the speed-dependent friction between surfaces—see Fig. 3(b). The results show a characteristic speed V_c beyond which the tangential force decreases dramatically. Such effects are consistent with the transition from the regime of solid-solid contact to that of mixed lubrication, that is commonly cited as part of the Stribeck diagram in tribology [14,39]. We have also confirmed that V_c is inversely proportional to the fluid viscosity, in consistence with prior literature [39].

We are now in a position to summarize our observations in a *state diagram*, shown as Fig. 3(c). The main plot contains multiple datasets with different combinations of volume fractions and fluid viscosity. We display the time-averaged shear stress σ_S as its vertical coordinate, over a

horizontal plane spanned by the mean normal stress σ_N and a dimensionless shear rate $d\dot{\gamma}/V_c$. Even without the full knowledge of the statistical distribution of interparticle speeds, one can anticipate that for state T to exhibit stick-slip behaviors, three conditions are necessary: (1) some of the particles must be in solid-solid contact (with a relative speed below V_c) to build up a highly stressed network. (2) Meanwhile, the spectrum of interparticle speeds should go across V_c , such that a fraction of the contacts are in the lubricated state, behaving as the “weak spots.” These weak spots migrate as the macroscopic shearing goes on and are likely to trigger a cascade of avalanche once they get a chance to percolate. (3) The number of solid-to-solid versus lubricated contacts should be comparable for the buildup and avalanche to reoccur with substantial amplitudes. Indeed, our data reveal that stick slip is prominent when $0.1 < (d\dot{\gamma}/V_c) < 1$. On one hand, when $(d\dot{\gamma}/V_c) \ll 1$, one could imagine that the number density of weak spots becomes too low, such that the system can only create sporadic, localized slips. In the other extreme, when $(d\dot{\gamma}/V_c) > 1$, the majority of contacts are lubricated such that stress buildup is prohibited such that the stress stays low. However, one can anticipate a nonmonotonic change as the viscous drag becomes dominant at higher shear rates and, far above the current scope of our experiments, shear thickening effects [13–16,20–22] might occur and demand descriptions by inertial numbers [40] instead.

Understandably, a clear separation between the regime dominated by solid-solid contacts and that by lubricated sliding demands a high volume fraction that warrants a network of load-bearing particles—in our case with $\phi > RLP$ [8]: we have verified by further data (Appendix E in Supplemental Material [28]) that, as ϕ goes below RLP , (a) the stick slip behaviors separating the two regimes mentioned above become undetectable, and that (b) at $\phi = 0.48$, $\sigma_S(\dot{\gamma})$ becomes monotonic and bears the appearance of the conventional flow curves, resembling what we have demonstrated previously with hydrogel particles in the same apparatus [41]. In Fig. 3(c), we use a diagram on the right to illustrate that the stick slips (the shaded area) disappear such that two regimes merge, once the system becomes a true suspension—with a low normal stress σ_N due to insufficient volume fractions which prevent the formation of a highly stressed packing. We find that the merging occurs with a viscous number $J = 10^{-6}$ and $d\dot{\gamma}/V_c \sim 0.3$. This observation is consistent with one recent work with a rotating drum [23] that reports a critical value $J_c \sim 10^{-6}$, below which smooth flows cease to exist. In fact, our experiments with grains packed in a fixed volume have extended the observations down to $J \sim 10^{-9}$ that is three decades below reported values in most stress-controlled experiments reviewed by Ref. [1]. The smallness of the new dimensionless parameter $d\dot{\gamma}/V_c$ provides a definition of “quasistatic solids.”

Interestingly, our discussions on how a dense granular pack ceases to be fluidic and enters the solidlike regime as

the driving rate decreases also shares many vocabularies with the BDH model proposed in 2011 [42]—see Appendix F in Supplemental Material [28] for a side-by-side comparison in the similarity and key differences.

Concluding remarks.—By recognizing the speed-dependent friction between particles, we establish a new dimensionless shear rate $d\dot{\gamma}/V_c$ for describing the solidlike behaviors that are not covered in existing paradigms based on the rheology of dense suspension. We find that (1) at high packing fractions, our data demonstrate a dangerous zone of shear rates exhibiting prominent stick slips, that provide an unambiguous signature to divide the solidlike regime (dominated by quasistatic contacts) and the fluidic regime (dominated by lubricated sliding); that (2) evidence from boundary force fluctuations combined with internal imaging reveals that such solid-fluid transition takes place in a continuous yet distinctive manner; and that (3) the transition is controlled by two parameters: driving rate and ϕ (or the stress σ_N), not just ϕ alone.

Our interpretations are distinguished from existing paradigms in three aspects. (A) We emphasize that the tangential force between contacting particles is sensitive to the relative speeds. Taking the speed distribution into account, one might see the system as having a mixture of high-versus low-friction contacts. To the best of the authors' knowledge, instabilities induced by *distributed* frictional coefficients have not yet been considered in most existing theories or models. In our opinion, this is essential to understanding systems in which velocity weakening is known to exist such as in earthquakes or quicksand. (B) The speed-dependent friction makes the packing fraction ϕ no longer the leading factor for the solid-fluid transition. (C) Features of the particle contacts are now considered in the dimensionless parameter we propose, unlike how they appear missing from previous paradigms such as in viscous number J . The regime changes are summarized in the state diagram we provide. We hope to inspire further interpretations from various points of view, such as a generalization from theories based on the percolations [10] or connections with elastoplastic models as shear rates are varied [43].

J.-C. Tsai acknowledges fruitful exchanges with Xiang Cheng, Joshua Dijksman, K.-T. Leung, C.-K. Chan, J.-R. Huang, H.-Y. Shih, and Nigel Goldenfeld over the manuscript, and supports of Institute of Physics, Academia Sinica, especially from Director Jason Chang and the Precision Machine Shop.

*Corresponding author.

jtsai@phys.sinica.edu.tw

[1] É. Guazzelli and O. Pouliquen, Rheology of dense granular suspensions, *J. Fluid Mech.* **852**, P1 (2018).

- [2] A. Nicolas, E. E. Ferrero, K. Martens, and J.-L. Barrat, Deformation and flow of amorphous solids: Insights from elastoplastic models, *Rev. Mod. Phys.* **90**, 045006 (2018).
- [3] I. S. Aranson, L. S. Tsimring, F. Malloggi, and E. Clément, Nonlocal rheological properties of granular flows near a jamming limit, *Phys. Rev. E* **78**, 031303 (2008).
- [4] D. L. Henann and K. Kamrin, Predictive, size-dependent continuum model for dense granular flows, *Proc. Natl. Acad. Sci. U.S.A.* **110**, 6730 (2013).
- [5] K.-L. Lee and F.-L. Yang, Relaxation-type nonlocal inertial-number rheology for dry granular flows, *Phys. Rev. E* **96**, 062909 (2017).
- [6] D. Bonn, M. M. Denn, L. Berthier, T. Divoux, and S. Manneville, Yield stress materials in soft condensed matter, *Rev. Mod. Phys.* **89**, 035005 (2017).
- [7] A. J. Liu and S. R. Nagel, Jamming is not just cool any more, *Nature (London)* **396**, 21 (1998).
- [8] L. E. Silbert, Jamming of frictional spheres and random loose packing, *Soft Matter* **6**, 2918 (2010).
- [9] D. Bi, J. Zhang, B. Chakraborty, and R. P. Behringer, Jamming by shear, *Nature (London)* **480**, 355 (2011).
- [10] T. Shen, C. S. O'Hern, and M. D. Shattuck, Contact percolation transition in athermal particulate systems, *Phys. Rev. E* **85**, 011308 (2012).
- [11] M. M. Bandi, M. K. Rivera, F. Krzakala, and R. E. Ecke, Fragility and hysteretic creep in frictional granular jamming, *Phys. Rev. E* **87**, 042205 (2013).
- [12] J. R. Royer and P. M. Chaikin, Precisely cyclic sand: Self-organization of periodically sheared frictional grains, *Proc. Natl. Acad. Sci. U.S.A.* **112**, 49 (2015).
- [13] E. Brown, N. A. Forman, C. S. Orellana, H. Zhang, B. W. Maynor, D. E. Betts, J. M. DeSimone, and H. M. Jaeger, Generality of shear thickening in dense suspensions, *Nat. Mater.* **9**, 220 (2010).
- [14] N. Fernandez, R. Mani, D. Rinaldi, D. Kadau, M. Mosquet, H. Lombois-Burger, J. Cayer-Barrioz, H. J. Herrmann, N. D. Spencer, and L. Isa, Microscopic Mechanism for Shear Thickening of Non-Brownian Suspensions, *Phys. Rev. Lett.* **111**, 108301 (2013).
- [15] C. Clavaud, A. Bérut, B. Metzger, and Y. Forterre, Revealing the frictional transition in shear-thickening suspensions, *Proc. Natl. Acad. Sci. U.S.A.* **114**, 5147 (2017).
- [16] R. Mari, R. Seto, J. F. Morris, and M. M. Denn, Shear thickening, frictionless and frictional rheologies in non-Brownian suspensions, *J. Rheol.* **58**, 1693 (2014).
- [17] C. H. Scholz, Earthquakes and friction laws, *Nature (London)* **391**, 37 (1998).
- [18] E. A. Jagla, F. P. Landes, and A. Rosso, Viscoelastic Effects in Avalanche Dynamics: A Key to Earthquake Statistics, *Phys. Rev. Lett.* **112**, 174301 (2014).
- [19] S. Ide, G. C. Beroza, D. R. Shelly, and T. Uchide, A scaling law for slow earthquakes, *Nature (London)* **447**, 76 (2007).
- [20] S. Jamali and J. F. Brady, Alternative Frictional Model for Discontinuous Shear Thickening of Dense Suspensions: Hydrodynamics, *Phys. Rev. Lett.* **123**, 138002 (2019).
- [21] V. Rathee, D. L. Blair, and J. S. Urbach, Localized stress fluctuations drive shear thickening in dense suspensions, *Proc. Natl. Acad. Sci. U.S.A.* **114**, 8740 (2017).

- [22] J. F. Morris, Shear thickening of concentrated suspensions: Recent developments and relation to other phenomena, *Annu. Rev. Fluid Mech.* **52**, 121 (2020).
- [23] H. Perrin, C. Clavaud, M. Wyart, B. Metzger, and Y. Forterre, Interparticle Friction Leads to Nonmonotonic Flow Curves and Hysteresis in Viscous Suspensions, *Phys. Rev. X* **9**, 031027 (2019).
- [24] M. Workamp and J. A. Dijksman, Contact tribology also affects the slow flow behavior of granular emulsions, *J. Rheol.* **63**, 275 (2019).
- [25] J.-C. Tsai, G. A. Voth, and J. P. Gollub, Internal Granular Dynamics, Shear-Induced Crystallization, and Compaction Steps, *Phys. Rev. Lett.* **91**, 064301 (2003).
- [26] J. A. Dijksman, F. Rietz, K. A. Lőrincz, M. van Hecke, and W. Losert, Invited article: Refractive index matched scanning of dense granular materials, *Rev. Sci. Instrum.* **83**, 011301 (2012).
- [27] The Dow Chemical, Sylgard-184.
- [28] See Supplemental Material at <http://link.aps.org/supplemental/10.1103/PhysRevLett.126.128001> for movies and full appendices A–F, which cover discussions over Refs. [29–33].
- [29] D. V. Denisov, K. A. Lőrincz, J. T. Uhl, K. A. Dahmen, and P. Schall, Universality of slip avalanches in flowing granular matter, *Nat. Commun.* **7**, 10641 (2016).
- [30] J. Antonaglia, W. J. Wright, X. Gu, R. R. Byer, T. C. Hufnagel, M. LeBlanc, J. T. Uhl, and K. A. Dahmen, Bulk Metallic Glasses Deform via Slip Avalanches, *Phys. Rev. Lett.* **112**, 155501 (2014).
- [31] E. DeGiuli and M. Wyart, Friction law and hysteresis in granular materials, *Proc. Natl. Acad. Sci. U.S.A.* **114**, 9284 (2017).
- [32] W. J. Wright, A. A. Long, X. Gu, X. Liu, T. C. Hufnagel, and K. A. Dahmen, Slip statistics for a bulk metallic glass composite reflect its ductility, *J. Appl. Phys.* **124**, 185101 (2018).
- [33] K. A. Dahmen, Y. Ben-Zion, and J. T. Uhl, Micromechanical Model for Deformation in Solids with Universal Predictions for Stress-Strain Curves and Slip Avalanches, *Phys. Rev. Lett.* **102**, 175501 (2009).
- [34] D. Lootens, H. Van Damme, and P. Hébraud, Giant Stress Fluctuations at the Jamming Transition, *Phys. Rev. Lett.* **90**, 178301 (2003).
- [35] J. H. Jensen, *Self-Organized Criticality: Emergent Complex Behavior in Physical and Biological Systems* (Cambridge University Press, Cambridge, England, 1998), Secs. 3.6 and 4.3.
- [36] J. H. Jensen, *Self-Organized Criticality: Emergent Complex Behavior in Physical and Biological Systems* (Ref. [35]), Sec. 5.2; also see M. LeBlanc, L. Angheluta, K. Dahmen, and N. Goldenfeld, *Phys. Rev. E* **87**, 022126 (2013).
- [37] J. H. Jensen, *Self-Organized Criticality: Emergent Complex Behavior in Physical and Biological Systems* (Ref. [35]), Sec. 3.2.
- [38] *Dynamical Heterogeneities in Glasses, Colloids, and Granular Media*, edited by L. Berthier, G. Biroli, J.-P. Bouchaud, L. Cipelletti, and W. van Saarloos (Oxford University Press, New York, 2011).
- [39] J. H. H. Bongaerts, K. Fourtouni, and J. R. Stokes, Soft-tribology: Lubrication in a compliant PDMS-PDMS contact, *Tribol. Int.* **40**, 1531 (2007); also see our work available at C.-E. Tsai and J.-C. Tsai, [arXiv:2010.07907](https://arxiv.org/abs/2010.07907) for further details.
- [40] Y. Forterre and O. Pouliquen, Flows of dense granular media, *Annu. Rev. Fluid Mech.* **40**, 1 (2008).
- [41] J.-C. Tsai, M.-R. Chou, P.-C. Huang, H.-T. Fei, and J.-R. Huang, *Soft Matter* (2020), <https://doi.org/10.1039/D0SM00405G>.
- [42] Y. Ben-Zion, K. A. Dahmen, and J. T. Uhl, A unifying phase diagram for the dynamics of sheared solids and granular materials, *Pure Appl. Geophys.* **168**, 2221 (2011).
- [43] C. Liu, E. E. Ferrero, F. Puosi, J.-L. Barrat, and K. Martens, Driving Rate Dependence of Avalanche Statistics and Shapes at the Yielding Transition, *Phys. Rev. Lett.* **116**, 065501 (2016).